Computers and Mathematics with Applications 123 (2022) 216–226

Contents lists available at ScienceDirect

Computers and Mathematics with Applications

www.elsevier.com/locate/camwa

Inverse two-phase nonlinear Stefan and Cauchy-Stefan problems: A phase-wise approach

P. Nanda [a,1], G.M.M. Reddy [a], M. Vynnycky [b,*]

[a] Department of Mathematics, BITS-Pilani Hyderabad Campus, Telangana, 500078, India

[b] Mathematics Applications Consortium for Science and Industry (MACSI), Department of Mathematics and Statistics, University of Limerick, Limerick, V94 T9PX, Ireland

ARTICLE INFO

Dataset link: https://codeocean.com/capsule/9072139/tree

Keywords:
Two-phase
Inverse Stefan problem
Boundary identification problem

ABSTRACT

We develop a novel phase-wise sequential numerical approach based on the method of fundamental solutions (MFS) for inverse two-phase nonlinear Stefan and Cauchy-Stefan problems in one dimension (1D). By treating each phase independently, the inverse two-phase nonlinear Stefan problem splits into two single-phase inverse problems: an inverse nonlinear boundary identification problem and an inverse linear one-phase Stefan problem. Along with the reconstruction of boundary data, the simultaneous reconstruction of the boundary and initial data is also considered. Numerical investigations show the robustness and efficiency of the proposed method in reconstructing the data.

1. Introduction

Stefan problems, in which a material solidifies or melts, occur in many situations in science and engineering [1–5]. Mathematically, these are particular cases of moving boundary problems, in which the position of the phase-change front is not known *a priori*, but needs to be determined simultaneously with the temperature field [6]. Such problems may themselves be categorized according to the number of distinct phases in which the temperature field must be solved for; in this paper, we are concerned with two-phase problems, as typically occur in casting processes [7–14], where the initial temperature of the melt is greater than the solidification temperature. Further recent examples of two-phase Stefan problems can be found in [15–17].

The references given above all refer to direct problems. On the other hand, in inverse two-phase Stefan problems, extra information, such as partial measurement of the moving interface position [6,18] or the temperature at selected interior points of the domain [19,20], is used to determine thermal properties and/or the initial and/or boundary conditions. Our interest is in a nonlinear variant of the Stefan problem that has an unknown moving boundary and overspecified data at one of the fixed boundaries. Such a problem has a unique solution; however, it is still ill-posed, as it is sensitive to a perturbation of the data [19].

Both the direct and inverse Stefan problems have been solved using different mesh-based numerical methods such as the finite-element method, the finite-difference method and the boundary-element method; for excellent expositions, we refer to [19]. However, the implementation of mesh-based methods can be computationally rather expensive, and a cheaper alternative is to use meshless methods, such as the method of fundamental solutions (MFS). Nevertheless, despite having a computational advantage over the classical mesh-based methods [21], MFS has scarcely been applied to inverse two-phase Stefan problems [22]; a possible reason for this is that it is difficult to know how to choose the MFS parameters, i.e. the location and number of source and collocation points and the regularization parameters, in such a way as to ensure a solution of a desired accuracy. In [23,24], an inverse two-phase linear Stefan problem was examined numerically using the MFS in one- and two-dimensions, respectively. Subsequently, the method was extended to a more complicated inverse two-phase nonlinear Stefan problem [22] in one dimension (1D). A common feature is to adopt an optimization technique where a nonlinear functional is minimized. In general, the functional is defined as the sum of squares of the discrepancies between the computed and given conditions with several regularization terms. One criticism of such an approach would be choosing the initial parameters to start the optimization process. Fur-

The code (and data) in this article has been certified as Reproducible by Code Ocean: https://codeocean.com/. More information on the Reproducibility Badge Initiative is available at https://www.elsevier.com/physical-sciences-and-engineering/computer-science/journals.

* Corresponding author.
E-mail address: michael.vynnycky@ul.ie (M. Vynnycky).
[1] Present address: Department of Statistics, Purdue University, 150 N. University St, West Lafayette, Indiana, 47907, USA.

https://doi.org/10.1016/j.camwa.2022.08.009
Received 28 December 2021; Received in revised form 18 June 2022; Accepted 5 August 2022

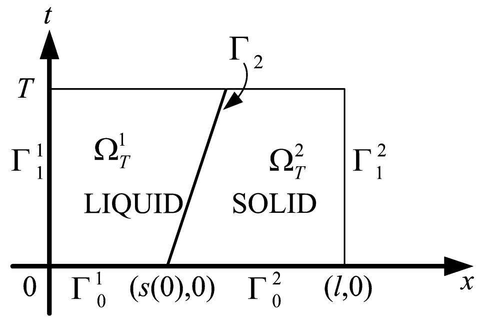

Fig. 1. Heat conduction domains, Ω_T^1 and Ω_T^2.

thermore, to obtain the regularization parameter, one has to rely on a trial-and-error approach [22]. This was the motivation for us to look for an alternative systematic strategy, as compared to the composite method proposed in [22].

The primary intent of this work is to adopt a linear discretization approach to solve the two-phase nonlinear inverse Stefan problem in 1D. We use the fact that the two-phase inverse Stefan problem [22] can be split into two ill-posed single-phase problems: an inverse nonlinear boundary identification problem and an inverse linear Stefan problem. The output of the boundary determination problem in one phase is treated as the input for the inverse Stefan problem in the other. Tikhonov regularization is used to counteract the high ill-conditioning of the MFS systems arising from each phase. Benchmark examples are tested to show the applicability of the proposed approach. To the best of our knowledge, there is no article in the literature embracing such a phase-wise approach to the inverse two-phase nonlinear Stefan problem, using the MFS or otherwise.

The article is organized as follows. The mathematical formulation of the two-phase nonlinear inverse Stefan problem is introduced in Section 2. Section 3 deals with the split methodology and the MFS discretizations. Section 4 is devoted to the numerical results and discussions. Finally, we draw conclusions in Section 5.

2. Problem statement

We begin this section by introducing the problem. As per the schematic in Fig. 1, let the heat conduction domain in the 1D setting be $\Omega_T = \{(x,t) : 0 < x < l, 0 < t \le T\}$, which is partitioned by the moving interface $x = s(t)$ $(0 < s(t) < l, t \in [0,T])$ into the liquid and solid phases given by

$$\Omega_T^1 = \{(x,t) : 0 < x < s(t),\ 0 < t \le T\},\ \text{and}$$

$$\Omega_T^2 = \{(x,t) : s(t) < x < l,\ 0 < t \le T\},$$

respectively, where T is the final time of interest. The fixed boundaries of Ω_T^1 and Ω_T^2 are represented as

$$\Gamma_1^1 = \{(0,t) : 0 < t \le T\} \quad \text{and} \quad \Gamma_1^2 = \{(l,t) : 0 < t \le T\}, \tag{1}$$

respectively, and the respective initial bases as

$$\Gamma_0^1 = \{(x,0) : 0 < x < s(0)\},\ \text{and}\ \Gamma_0^2 = \{(x,0) : s(0) < x < l\}.$$

Γ_2 denotes the free boundary that separates the liquid and the solid phases, where

$$\Gamma_2 = \{(s(t),t) : 0 < t \le T\}.$$

Note that the initial position of the moving boundary, $s(0)$, is assumed to be known.

Let $\alpha_k, k = 1,2$, denote the thermal diffusivities, assumed constant, of the heat-conducting regions $\Omega_T^k, k = 1,2$, respectively. Then, the direct two-phase nonlinear Stefan problem comprises of obtaining the triplet

$$(u_1,u_2,s) \in C^{2,1}(\Omega_T^1) \times C^{2,1}(\Omega_T^2) \times (C[0,T] \cap C^1(0,T])$$

satisfying the governing equations,

$$\frac{\partial u_k}{\partial t} = \alpha_k \frac{\partial^2 u_k}{\partial x^2},\ (x,t) \in \Omega_T^k,\ k = 1,2, \tag{2}$$

subject to: the initial conditions,

$$u_1(x,0) = \varphi_1(x),\ \ x \in [0,s(0)], \tag{3}$$

$$u_2(x,0) = \varphi_2(x),\ \ x \in [s(0),l]; \tag{4}$$

on Γ_1^1, the Dirichlet condition,

$$u_1(0,t) = \phi_1(t),\ \ t \in (0,T], \tag{5}$$

or the Neumann condition

$$-k_1 \frac{\partial u_1}{\partial x}(0,t) = \psi_1(t),\ \ t \in (0,T], \tag{6}$$

where k_1 is a positive constant; Dirichlet conditions on the moving interface Γ_2,

$$u_1(s(t),t) = u_2(s(t),t) = u^*(t),\ \ t \in (0,T]; \tag{7}$$

the Stefan condition on the moving interface Γ_2,

$$K_2 \frac{\partial u_2}{\partial x}(s(t),t) - K_1 \frac{\partial u_1}{\partial x}(s(t),t) = \frac{\mathrm{d}s}{\mathrm{d}t},\ \ t \in (0,T], \tag{8}$$

where K_1 and K_2 are positive constants; and, on Γ_1^2, the Dirichlet condition,

$$u_2(l,t) = \phi_2(t),\ \ (l,t) \in \Gamma_1^2, \tag{9}$$

or the Neumann condition,

$$k_2 \frac{\partial u_2}{\partial x}(l,t) = \psi_2(t),\ \ (l,t) \in \Gamma_1^2, \tag{10}$$

where k_2 is a positive constant. In addition, we require the following conditions so as to ensure compatibility between the initial and boundary conditions at $t = 0$:

$$\phi_1(0) = \varphi_1(0), \tag{11}$$

$$\psi_1(0) = -k_1 \frac{\mathrm{d}\varphi_1}{\mathrm{d}x}(0), \tag{12}$$

$$u^*(0) = \varphi_1(s(0)) = \varphi_2(s(0)), \tag{13}$$

$$\phi_2(0) = \varphi_2(l), \tag{14}$$

$$\psi_2(0) = k_2 \frac{\mathrm{d}\varphi_2}{\mathrm{d}x}(l). \tag{15}$$

For the direct problem, depending upon the prescribed boundary conditions, we assume the compatibility conditions either (11) or (12), (13), and either (14) or (15). For the well-posedness of these problems, we refer to [19]. In this article, we are interested in investigating a standard inverse two-phase nonlinear Stefan problem, where the boundary conditions on Γ_1^1 are not prescribed and must be reconstructed, along with the temperature distributions and the location of the moving boundary using some overspecified data at $x = l$. Precisely, we are interested in solving the inverse problem satisfying equations (2)-(4) and (7)-(10), assuming that the compatibility conditions (11)-(15) are satisfied.

Although the topic of interest may be considered as a continuation problem of the solution to the parabolic equation from the boundary $x = l$ into the domain Ω_T, it is much more complicated than the non-characteristic Cauchy problem due to the unknown moving phase transition boundary in Ω_T [19]. This inverse problem has a unique solution; however, it is sensitive to the perturbations in the input data [25]. Further, since the initial conditions (3) and (4) are not necessary for the inverse problem to have a unique solution [22,26], we also try to retrieve the boundary as well as the initial data simultaneously by solving the inverse problem given by equations (2), (7)-(10) and respective compatibility conditions; this is commonly referred to as an inverse Cauchy-Stefan problem. As in [22], noise will be induced only in the Dirichlet condition (9). Thus, in the inverse formulation, we prescribe the following Dirichlet data:

$$u_2(l,t)=\phi_2^{\delta}(t),\ \ (l,t)\in\Gamma_1^2, \tag{16}$$

where δ denotes the percentage of added noise.

3. Methodology

We begin this section by introducing the fundamental solutions.

3.1. The MFS

The fundamental solutions for the heat equations governing the temperature distribution on the two phases can be expressed as

$$F_k(x,t;z,\tau)=\frac{H(t-\tau)}{\sqrt{4\pi\alpha_k(t-\tau)}}\exp\left\{-\frac{(x-z)^2}{4\alpha_k(t-\tau)}\right\}, \tag{17}$$

where $k=1,2,\ x,z\in\mathbb{R}$. Thus, the analytic solutions $u_k,\ k=1,2$ to the heat equations can be approximated by the linear combinations of the respective fundamental solutions and are given by

$$u_{k_{MFS}}(x,t)=\sum_{i=1}^{2}\sum_{j=1}^{N}c_{i,j}^{k}F_k(x,t;z_i^k,\tau_j),\ \ (x,t)\in\Omega_T^1,\ \ k=1,2, \tag{18}$$

where $(z_i^k,\tau_j)\in\mathbb{R}^2,\ i=1,2,\ j=1,2,\dots,N,\ k=1,2$, for some $N\in\mathbb{N}$, are the source points arranged on pseudo-boundaries on both sides of the respective phases. The problem on each phase now boils down to finding the unknown coefficients $c_{i,j}^1$, and $c_{i,j}^2,\ i=1,2,\ j=1,2,\dots,N$, by solving a linear system of equations arising as a result of collocating the boundary and initial conditions with some suitable arrangement of source points.

3.2. A phase-wise split approach

In this work, we adopt a two-step strategy that enables us to consider the two phases separately. In the first step, it is required to solve a nonlinear inverse boundary identification problem, involving equation (2) for the second phase, (4), (16), (10), compatibility conditions (14) and (15), and $u_2(s(t),t)=u^*(t), t\in(0,T]$ with $u^*(0)=\varphi_2(s(0))$, in order to obtain the temperature distribution in the solid region, u_2, along with the location of the moving boundary, s. This problem has a unique solution [27], even if the initial data is not specified; see [28,29]. The second step uses the obtained approximate for s to solve a one-phase linear inverse Stefan problem that satisfies equation (2) for the first phase, (3), (7), (8), and $u^*(0)=\varphi_1(s(0))$. Also, this problem has a unique solution [26], even in the absence of the initial data [30,31]. Both of these problems are ill-posed, as they are sensitive to input data, and hence we use Tikhonov regularization to restore stability.

For a given amount of noise induced in the boundary data on $x=l$, we first obtain the approximations $u_{2_{MFS}}^{\theta}$ and s_{MFS}^{θ} to the solid temperature distribution and the moving interface, respectively. Here, θ is an indication of the deviation of the approximations from the exact solutions. For the estimated s_{MFS}^{θ}, we are going to solve a linear inverse problem on a perturbed domain $\Omega_T^{1,\theta}$ instead of the actual domain Ω_T^1. A likely scenario is $u_1(s_{MFS}^{\theta}(t),t)\not\equiv 0,\ t\in(0,T]$. Thus, imposing the conditions (7) and (8) on s_{MFS}^{θ} essentially induces noise into the computation of the liquid temperature distribution $u_{1_{MFS}}^{\epsilon}$ with an error ϵ. Thus, an initial attempt would be to make s_{MFS}^{θ} as accurate as possible, and it is expected that as $\theta\to 0$, we have $\epsilon\to 0$. So, the computations on the liquid phase are performed, taking the best possible approximations from the solid phase. The systems of equations resulting from the collocation of given data on both phases are ill-conditioned. Hence, instead of solving the original systems of equations, we solve the regularized ones.

3.3. Source and collocation points

To begin with, we discuss the schemes for arranging the source and collocation points when the initial conditions are provided. For a given $M\in\mathbb{N}$, the number of source points for any phase is $4M$. To this end, the time axis has been discretized as

$$\tau_j=\frac{2(j-M)-1}{2M}T,\ \ j=1,\dots,2M.$$

Then, the source points sandwiching the solid phase are at

$$(s(0)-h,\tau_j),\ \ j=1,\dots,2M\quad\text{and}\quad(l+h,\tau_j),\ \ j=1,\dots,2M;$$

similarly, for the liquid phase, the source points are placed at

$$(-h,\tau_j),\ \ j=1,\dots,2M\quad\text{and}\quad(s(0)+h,\tau_j),\ \ j=1,\dots,2M.$$

For collocating the given conditions, the temporal discretization is

$$t_i=\frac{i}{M+1}T,\ \ i=1,\dots,M,$$

on both the phases, whilst the spatial discretization is, for the liquid phase,

$$x_k^1=\frac{k}{2M}s(0),\ \ k=1,\dots,2M,$$

and, for the solid phase,

$$x_k^2=s(0)+\frac{k(l-s(0))}{2M},\ \ k=1,\dots,2M.$$

Thus, for the solid phase, the Dirichlet and Neumann data on the boundary $x=l$ are prescribed at the points $(l,t_i),\ i=1,\dots,M$, and the initial condition at $(x_k^2,0),\ k=1,\dots,2M$. For the liquid phase, the interface temperature and flux conditions are collocated at $(s_{MFS}(t_i),t_i)$, $i=1,\dots,M$, and the initial condition (3) at $(x_k^1,0),\ k=1,\dots,2M$, where s_{MFS} is the MFS approximation of the moving interface. A schematic is shown in Fig. 2.

When the initial conditions are not provided, in which case we have an inverse Cauchy-Stefan problem, the scheme of placing the source points has not been altered. However, changes have been made to the arrangement of collocation points. The boundary data (10) and (16) are collocated at the points $(l,t_j),\ j=1,\dots,2M$, where $t_j=jT/(2M+1)$, $j=1,\dots,2M$. Analogously, the interface conditions are collocated at the points $(s_{MFS}(t_j),t_j),\ j=1,\dots,2M$. We note that the discretizations are such that for a given $M\in\mathbb{N}$, the number of collocation points is the same as that of the source points for each phase. The schematic for this case is shown in Fig. 3.

3.4. MFS systems of equations

The collocation of the given boundary data on Γ_1^2 and the initial condition on Γ_0^2 generates the following system of equations:

$$u_{2_{MFS}}(l,t_i)=\phi_2^{\delta}(t_i),\ \ i=1,\dots,M, \tag{19}$$

$$k_2\frac{\partial u_{2_{MFS}}}{\partial x}(l,t_i)=\psi_2(t_i),\ \ i=1,\dots,M, \tag{20}$$

$$u_{2_{MFS}}(x_k^2,0)=\varphi_2(x_k^2),\ \ k=1,\dots,2M. \tag{21}$$

In the computations, for a given M, the noisy data (16) have been synthesized in the following manner:

$$\phi_2^{\delta}(t_i)=\phi_2(t_i)+\left(\delta\times\max_i\phi_2(t_i)\times N(0,1)\right),\ \ i=1,\dots,M, \tag{22}$$

where δ denotes the relative percentage of noise and $N(0,1)$ denotes a random number drawn from the standard Gaussian distribution. This $(4M\times 4M)$ system of equations can be rewritten as $\mathbf{A}_2\mathbf{c}_2=\mathbf{f}_2$, where $\mathbf{A}_2$ is the matrix containing the values of the fundamental solution F_2 evaluated for all possible combinations of the source and collocation points, $\mathbf{c}_2=\{c_{i,j}^2\}$ and $\mathbf{f}_2$ is the vector of collocated boundary data and

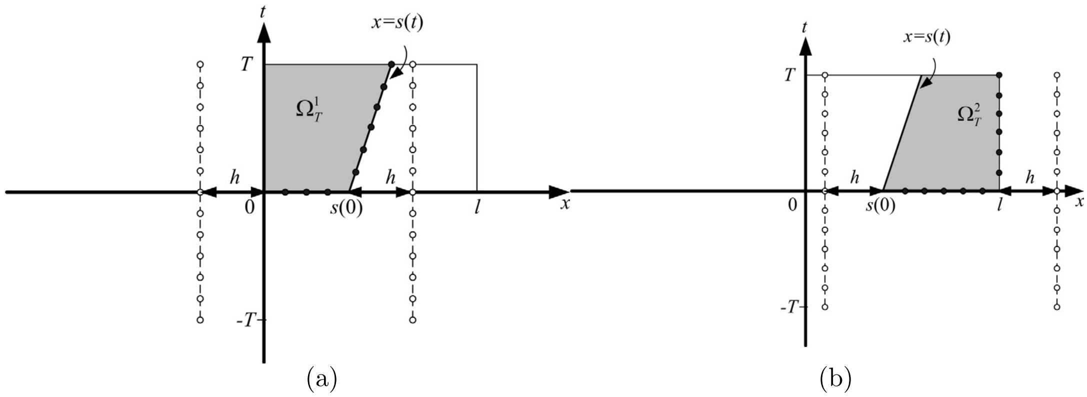

Fig. 2. Distribution of source (–○–) and collocation (–●–) points for the inverse Stefan problem for: (a) the liquid region; (b) the solid region.

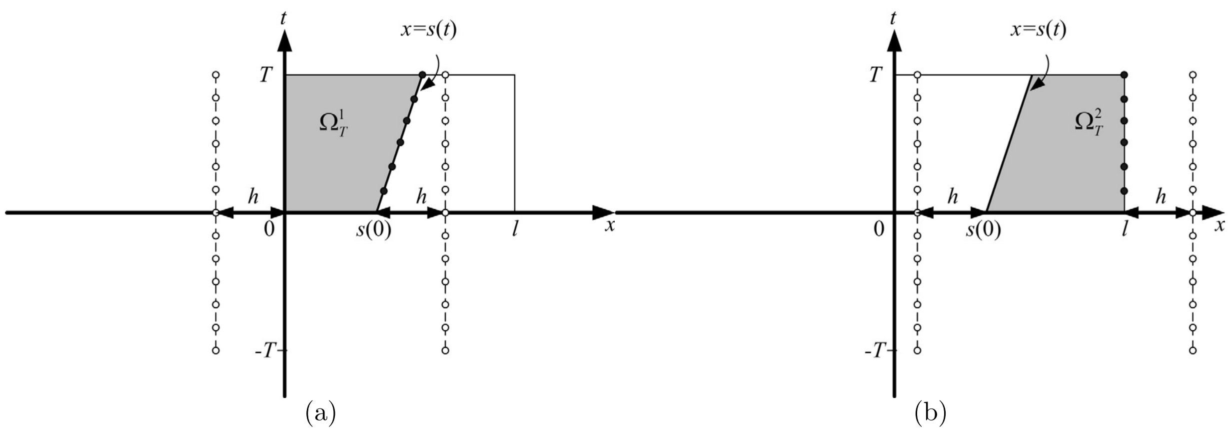

Fig. 3. Distribution of source (–○–) and collocation (–●–) points for the inverse Cauchy-Stefan problem for: (a) the liquid region; (b) the solid region.

initial condition. The above ill-conditioned system is transformed using Tikhonov regularization into

$$(\mathbf{A}_2^t\mathbf{A}_2 + \lambda_2\mathbf{I})\mathbf{c}_2 = \mathbf{A}_2^t\mathbf{f}_2, \tag{23}$$

where the superscript 't' denotes the transpose and λ_2 is the regularization parameter. Subsequently, the MFS approximation, s_{MFS}, of the moving interface at each time level t_i is determined by solving $u_{2_{MFS}}(x,t_i)=0$ for $x=s_{MFS}(t_i)$, $i=1,\dots,M$. Next, the interface conditions are collocated at the points $(s_{MFS}(t_i),t_i)$ and the initial condition at $(x_k^1,0)$, as a result of which we have the following system of equations for the liquid phase:

$$u_{1_{MFS}}(s_{MFS}(t_i),t_i)=0,\ \ i=1,\dots,M, \tag{24}$$

$$\frac{\partial u_{1_{MFS}}}{\partial x}(s_{MFS}(t_i),t_i)=\frac{1}{K_1}\left\{K_2\frac{\partial u_{2_{MFS}}}{\partial x}(s_{MFS}(t_i),t_i)-\frac{\mathrm{d}s_{MFS}}{\mathrm{d}t}(t_i)\right\},\quad i=1,\dots,M, \tag{25}$$

$$u_{1_{MFS}}(x_k^1,0)=\varphi_1(x_k^1),\ \ k=1,\dots,2M. \tag{26}$$

Again, we have a $(4M\times 4M)$ system of equations which can be represented as $\mathbf{A}_1\mathbf{c}_1=\mathbf{f}_1$, and be further regularized to yield

$$(\mathbf{A}_1^t\mathbf{A}_1 + \lambda_1\mathbf{I})\mathbf{c}_1 = \mathbf{A}_1^t\mathbf{f}_1, \tag{27}$$

where $\mathbf{A}_1$, $\mathbf{c}_1$, and $\mathbf{f}_1$ are the analogous versions of $\mathbf{A}_2$, $\mathbf{c}_2$, and $\mathbf{f}_2$, respectively, in the liquid phase. The regularized systems (23) and (27) are solved using the Gaussian elimination method. The solution procedure remains the same for the case when we are not provided with the initial conditions, i.e. the inverse Cauchy-Stefan problem. However, the systems of equations will change according to the collocated data in the two phases.

4. Numerical investigation

This section investigates two of the benchmark problems that were considered in [22]. Before that, we discuss a sequential optimization algorithm that facilitates the computation of the optimal MFS approximations, as well our experience of the computational cost in using it. All computations were carried out using an Intel(R) Core(TM) i5-10210U CPU @ 1.60 GHz 2.10 GHz processor and 8.00 GB of RAM.

4.1. Set-up for numerical experiments

We extend the algorithms in [32–34] to optimize $u_{2_{MFS}}$ and then $u_{1_{MFS}}$ sequentially. Let $\mathcal{N}$, h, and λ denote the number of source points, the distance of the pseudo-boundaries, and the regularization parameter, respectively. Further, let $\mathcal{N}_{min}$, h_{min}, and λ_{min} denote minimum values of $\mathcal{N}$, h, and λ, respectively. Similarly, $\mathcal{N}_{max}$, h_{max}, and λ_{max} denote the corresponding maximum values for these parameters. Within the respective ranges, the parameters $\mathcal{N}$, h, and λ take on values with increments $\mathcal{N}_{step}$, h_{step}, and λ_{step}, respectively. In the computations, these variables have been chosen as: $\mathcal{N}_{min}=12$, $\mathcal{N}_{max}=80$, $\mathcal{N}_{step}=4$, $h_{min}=1.0$, $h_{max}=2.5$, $h_{step}=0.1$, $\lambda_{min}=10^{-16}$, $\lambda_{max}=10^{-1}$, and $\lambda_{step}=10$ (multiplicative increment). In order to disambiguate when comparing our results with those in [22], $(\mathcal{N}_i^*, h_i^*, \lambda_i^*)$, $i=1,2$ will denote the optimized parameters in phase i using our method, whereas $(\mathcal{N}_i, h_i, \lambda_i)$, $i=1,2$ will denote the parameters used to generate the results in [22].

The optimization process essentially follows two steps. The first step determines the optimal values of the MFS parameters for the solid phase by optimizing $u_{2_{MFS}}$ over the specified range of parameters. The optimized $u_{2_{MFS}}$ will then be used to trace the location of the moving interface, s_{MFS}. In the next step, optimizing $u_{1_{MFS}}$ over the specified

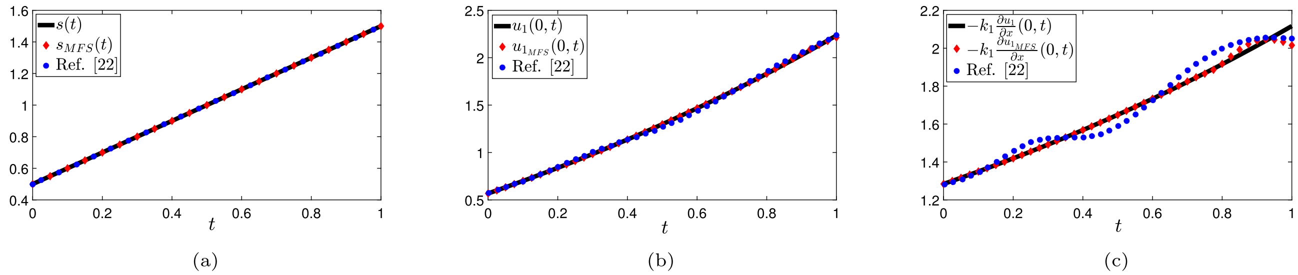

Fig. 4. Approximations obtained for Example 1 and $\delta = 0$, when the initial conditions (3) and (4) are prescribed. $\mathcal{N}_2^* = 76$, $h_2^* = 2.1$, $\lambda_2^* = 10^{-16}$, $\mathcal{N}_1^* = 60$, $h_1^* = 2.1$, $\lambda_1^* = 10^{-11}$. The approximations in [22] were obtained with $\mathcal{N}_1 = \mathcal{N}_2 = 80$, $h_1 = h_2 = 3$, $\lambda_1 = \lambda_2 = 0$. The total number of collocation points therein is 224.

Algorithm 1 A phase-wise optimization algorithm for the nonlinear inverse two-phase Stefan problem.

Input: $\mathcal{N}_{min}, \mathcal{N}_{step}, \mathcal{N}_{max}, h_{min}, h_{step}, h_{max}, \lambda_{min}, \lambda_{step}, \lambda_{max}, \delta$
Output: $\mathcal{N}_1^*, h_1^*, \lambda_1^*, \mathcal{N}_2^*, h_2^*, \lambda_2^*$
for $\mathcal{N} \leftarrow \mathcal{N}_{min} : \mathcal{N}_{step} : \mathcal{N}_{max}$ **do**
  for $h \leftarrow h_{min} : h_{step} : h_{max}$ **do**
    for $\lambda \leftarrow \lambda_{min} : \lambda_{step} : \lambda_{max}$ **do**
      Compute $u_{2_{MFS}}(x,t;\mathcal{N},h,\lambda)$ by solving equation (23)
      $\mathbf{e}_{u_2}(\mathcal{N},h,\lambda) \leftarrow \|u_{2_{MFS}}(x,t;\mathcal{N},h,\lambda) - u_2(x,t)\|_{\Omega_T^2}$
    end for
  end for
end for
$\mathbf{e}_{u_2}(\mathcal{N}_2^*,h_2^*,\lambda_2^*) \leftarrow \min_{\mathcal{N},h,\lambda} \mathbf{e}_{u_2}(\mathcal{N},h,\lambda)$
Solve $u_{2_{MFS}}(x,t;\mathcal{N}_2^*,h_2^*,\lambda_2^*) = 0$ for $x = s_{MFS}(t;\mathcal{N}_2^*,h_2^*,\lambda_2^*)$
for $\mathcal{N} \leftarrow \mathcal{N}_{min} : \mathcal{N}_{step} : \mathcal{N}_{max}$ **do**
  for $h \leftarrow h_{min} : h_{step} : h_{max}$ **do**
    for $\lambda \leftarrow \lambda_{min} : \lambda_{step} : \lambda_{max}$ **do**
      Compute $u_{1_{MFS}}(x,t;\mathcal{N},h,\lambda)$ using $s_{MFS}(t;\mathcal{N}_2^*,h_2^*,\lambda_2^*)$ in equation (27).
      $\mathbf{e}_{u_1}(\mathcal{N},h,\lambda) \leftarrow \|u_{1_{MFS}}(x,t;\mathcal{N},h,\lambda) - u_1(x,t)\|_{\Omega_T^1}$
    end for
  end for
end for
$\mathbf{e}_{u_1}(\mathcal{N}_1^*,h_1^*,\lambda_1^*) \leftarrow \min_{\mathcal{N},h,\lambda} \mathbf{e}_{u_1}(\mathcal{N},h,\lambda)$

range of the MFS parameters gives the estimated optimal values for the liquid phase.

4.2. Computational cost

With respect to $\mathcal{N}_{step}$, in the computations for either of the two phases, the value of $\mathcal{N}$ was incremented by four. These four points are uniformly distributed around the solution domain for the particular phase: one in each of the four quadrants. We experimented with different kinds of distributions/increments of the source points, and came to the conclusion that a uniform distribution/increment scheme is more likely to give better accuracy. Thus, adding fewer than four source points at each iteration is less likely to produce a better reconstruction. However, if we add eight new points at each iteration, i.e. two in each quadrant, then the jump in the $\mathcal{N}$ value is greater, and hence the algorithm may skip optimal values of $\mathcal{N}$.

As regards h_{step}, we noted that taking $h_{step} < 0.1$ greatly increased the computational cost. However, the numerical experiments did not show any significant improvement in the reconstructed data if h_{step} were taken to be very small, as the desired results are already of the order of the noise. To reduce the computational time of the algorithm, one may take a small risk and go with $h_{step} = 0.2$; however, increasing h_{step} further may skip optimal values of h. Therefore, taking $h_{step} = 0.1$ seemed reasonable.

As for λ_{step}, the value used is quite a standard one that has been used in our own earlier work, as well as in that of others. Moreover, computations with a smaller value of λ_{step} tend to be computationally expensive without any appreciable improvement in the results.

4.3. Examples

4.3.1. Example 1

The coefficients in the heat equations are given as $\alpha_1 = 2$ and $\alpha_2 = 1$, and those in the interface-flux condition as $K_1 = 2$ and $K_2 = 1$. The final time level and the fixed boundary of the solid phase are at $T = 1$ and $l = 2$, respectively. In addition, the coefficients in the Neumann conditions (6) and (10) are taken as $k_1 = 1$ and $k_2 = 2$, respectively. The exact temperature distribution in the liquid phase is determined by

$$u_1(x,t) = 2\left(\exp\left(\frac{t+0.5-x}{2}\right) - 1\right), \quad (x,t) \in \Omega_T^1, \tag{28}$$

and that in the solid phase by

$$u_2(x,t) = \exp(t+0.5-x) - 1, \quad (x,t) \in \Omega_T^2. \tag{29}$$

The exact location of the moving interface that separates the two phases can be expressed as

$$s(t) = t + 0.5, \quad t \in [0,T]. \tag{30}$$

The boundary conditions to be reconstructed are derived from equation (28) as

$$u_1(0,t) = 2\left(\exp\left(\frac{t+0.5}{2}\right) - 1\right), \quad -k_1\frac{\partial u_1}{\partial x}(0,t) \quad = k_1 \exp\left(\frac{t+0.5}{2}\right). \tag{31}$$

To synthesize the boundary data $\phi_2^\delta(t)$, $u_2(l,t)$ has been contaminated with random noise as shown in equation (22).

For $\delta = 0$, Figs. 4a, 4b, and 4c present, respectively, the MFS approximations (indicated in red) to the moving interface, the Dirichlet condition (5), and the Neumann condition (6). For the purposes of comparison, approximations from [22] are included in the plots, and indicated in blue. Optimized $(\mathcal{N}, h, \lambda)$-combinations determined by the proposed algorithm, along with the MFS parameters chosen in [22], are listed in the captions to each figure. The aforementioned reconstructions are presented in Figs. 5 and 6 in the case of noisy data.

As discussed in Section 2, the initial conditions (3) and (4) are unnecessary for the inverse problem to have a unique solution. Thus, in the next step, we solved the inverse problem given by (2), (7), (8), (10), (16), i.e., when the initial conditions (3) and (4) are not prescribed. We recovered the initial data on $\Gamma_0^1 \cup \Gamma_0^2$, along with the boundary data on $x = 0$ and the estimated location of the moving boundary. These reconstructed data (in red) are compared with the corresponding ones from [22] (in blue) in Figs. 7, 8, and 9 for the cases of $\delta = 0$, $\delta = 1\%$, and $\delta = 5\%$, respectively. Note that for both of the test problems, the MFS approximation to the initial data has been plotted over the complete range $(0, l)$ instead of over $(0, s(0))$ and $(s(0), l)$ separately. Therefore, instead of using separate notation for the two phases, we indicate the exact and reconstructed initial data by $u(x,0)$ and $u_{MFS}(x,0)$, respectively.

Finally, we point out that it appears that the approximations for the heat flux obtained in [22] were made using $k_1 = 2$, instead of $k_1 = 1$, which was the original authors' intended value. Thus, in plotting the blue curves in Figs. 4c-9c, we have made the requisite adjustment, in order to allow a fair comparison.

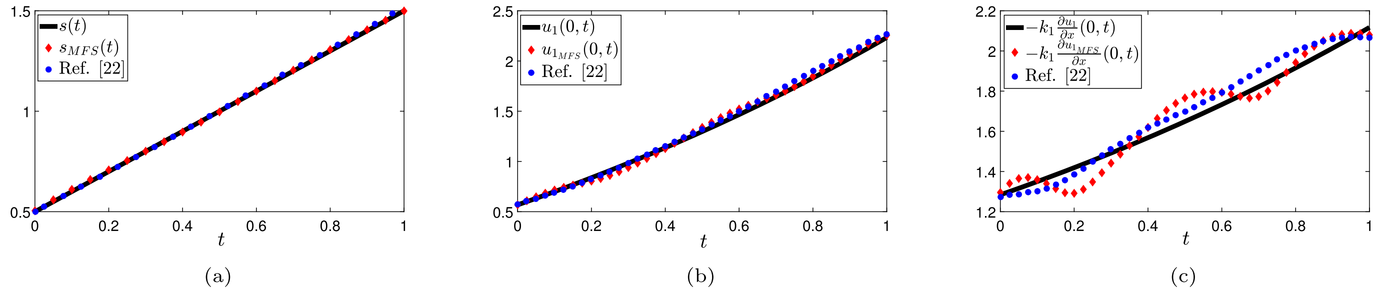

Fig. 5. Approximations obtained for Example 1 and $\delta = 1\%$, when the initial conditions (3) and (4) are prescribed. $\mathcal{N}_2^* = 64$, $h_2^* = 1.6$, $\lambda_2^* = 10^{-5}$, $\mathcal{N}_1^* = 24$, $h_1^* = 2.5$, $\lambda_1^* = 10^{-10}$. The approximations in [22] were obtained with $\mathcal{N}_1 = \mathcal{N}_2 = 40$, $h_1 = h_2 = 3$, $\lambda_1 = \lambda_2 = 10^{-6}$. The total number of collocation points therein is 114.

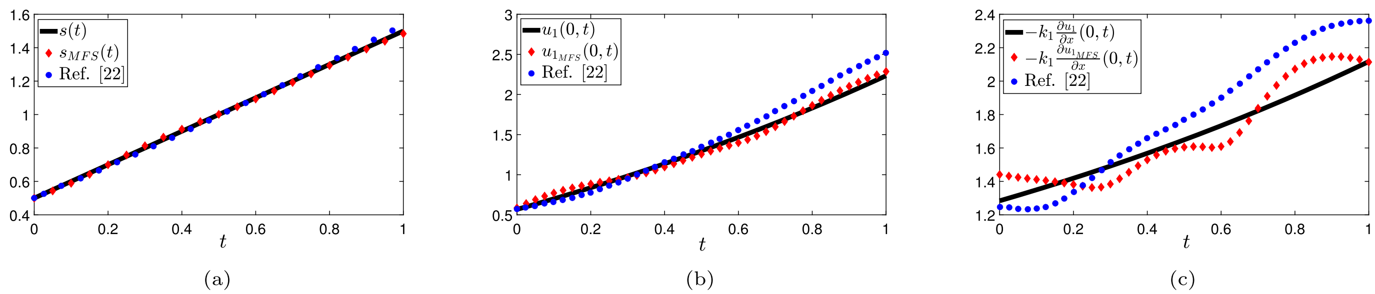

Fig. 6. Approximations obtained for Example 1 and $\delta = 5\%$, when the initial conditions (3) and (4) are prescribed. $\mathcal{N}_2^* = 60$, $h_2^* = 1.6$, $\lambda_2^* = 10^{-5}$, $\mathcal{N}_1^* = 12$, $h_1^* = 2.5$, $\lambda_1^* = 10^{-7}$. The approximations in [22] were obtained with $\mathcal{N}_1 = \mathcal{N}_2 = 40$, $h_1 = h_2 = 3$, $\lambda_1 = \lambda_2 = 10^{-6}$. The total number of collocation points therein is 114.

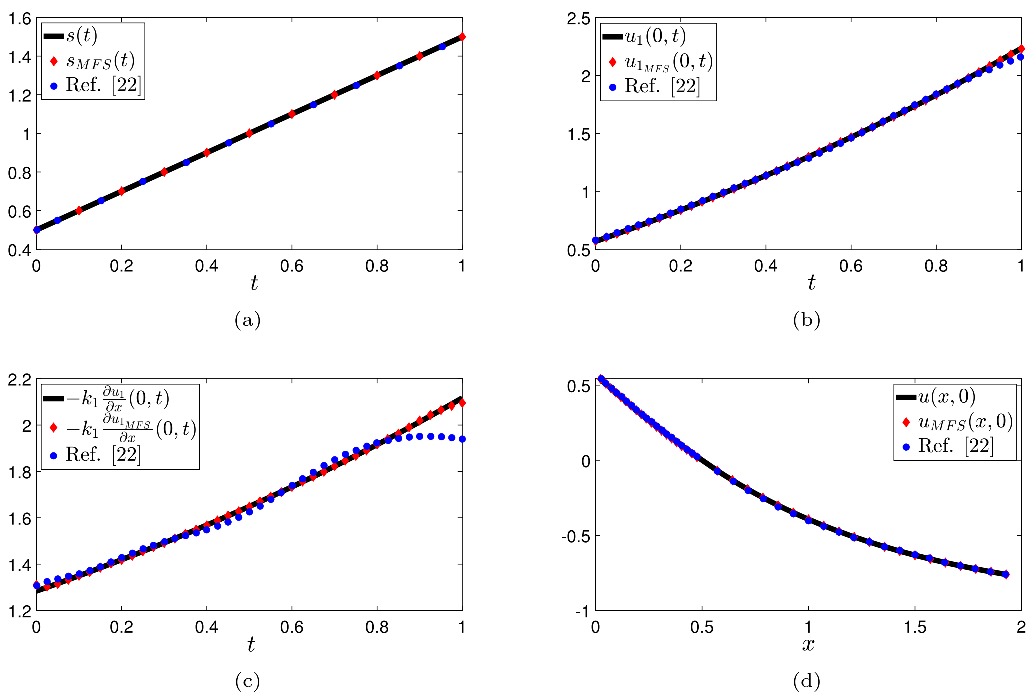

Fig. 7. Approximations obtained for Example 1 and $\delta = 0$, when the initial conditions (3) and (4) are not prescribed. $\mathcal{N}_2^* = 76$, $h_2^* = 2.0$, $\lambda_2^* = 10^{-15}$, $\mathcal{N}_1^* = 44$, $h_1^* = 2.1$, $\lambda_1^* = 10^{-13}$. The approximations in [22] were obtained with $\mathcal{N}_1 = \mathcal{N}_2 = 40$, $h_1 = h_2 = 3$, $\lambda_1 = \lambda_2 = 0$. The total number of collocation points therein is 114.

4.3.2. Example 2

The parameters for this benchmark are given as $l = 1$, $\alpha_1 = 0.5$, $\alpha_2 = 1$, $k_1 = 0.5$, $k_2 = 1$, $K_1 = 0.5$, and $K_2 = 1$. The analytical solution for this set of parameters is given by

$$u_1(x,t) = 1 - \frac{\mathrm{erf}\left(\frac{x}{2\sqrt{\alpha_1(t+t_0)}}\right)}{\mathrm{erf}\left(\frac{\gamma}{2\sqrt{\alpha_1}}\right)}, \quad (x,t) \in \Omega_T^1, \tag{32}$$

$$u_2(x,t) = -1 + \frac{\mathrm{erfc}\left(\frac{x}{2\sqrt{\alpha_2(t+t_0)}}\right)}{\mathrm{erfc}\left(\frac{\gamma}{2\sqrt{\alpha_2}}\right)}, \quad (x,t) \in \Omega_T^2, \tag{33}$$

$$s(t) = \gamma\sqrt{t+t_0}, \quad t \in [0,T], \tag{34}$$

where $\gamma = 0.479611$ and $t_0 = 0.695571$; in addition, erf denotes the error function and is given by

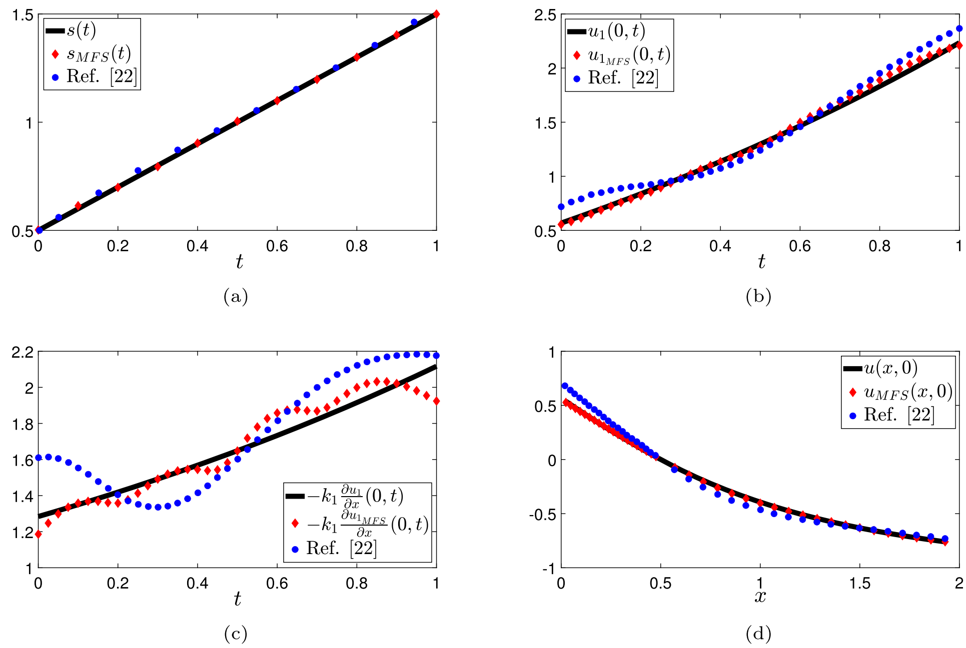

Fig. 8. Approximations obtained for Example 1 and $\delta = 1\%$, when the initial conditions (3) and (4) are not prescribed. $\mathcal{N}_2^* = 56$, $h_2^* = 1.1$, $\lambda_2^* = 10^{-5}$, $\mathcal{N}_1^* = 16$, $h_1^* = 2.1$, $\lambda_1^* = 10^{-5}$. The approximations in [22] were obtained with $\mathcal{N}_1 = \mathcal{N}_2 = 40$, $h_1 = h_2 = 3$, $\lambda_1 = \lambda_2 = 10^{-6}$. The total number of collocation points therein is 114.

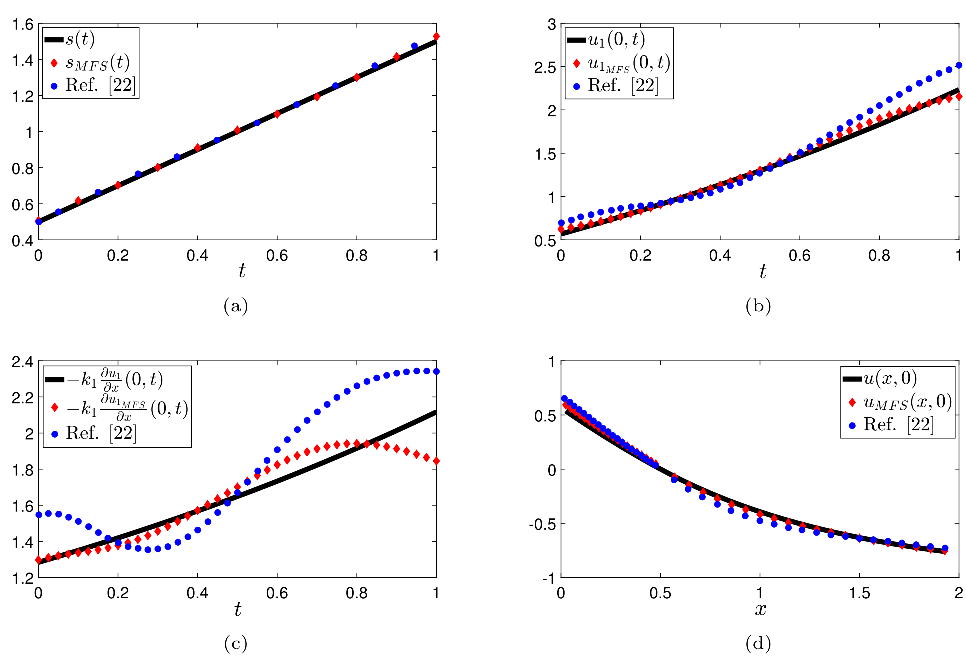

Fig. 9. Approximations obtained for Example 1 and $\delta = 5\%$, when the initial conditions (3) and (4) are not prescribed. $\mathcal{N}_2^* = 56$, $h_2^* = 1.4$, $\lambda_2^* = 10^{-5}$, $\mathcal{N}_1^* = 60$, $h_1^* = 2.5$, $\lambda_1^* = 10^{-3}$. The approximations in [22] were obtained with $\mathcal{N}_1 = \mathcal{N}_2 = 40$, $h_1 = h_2 = 3$, $\lambda_1 = \lambda_2 = 10^{-6}$. The total number of collocation points therein is 114.

$$\operatorname{erf}(z) = \frac{2}{\sqrt{\pi}} \int_0^z e^{-z^2}\,\mathrm{d}z,$$

and erfc denotes the complementary error function and is given by $\operatorname{erfc}(z) = 1 - \operatorname{erf}(z)$. The boundary conditions to be reconstructed are derived from equation (32) as

$$u_1(0,t) = 1, \quad -k_1 \frac{\partial u_1}{\partial x}(0,t) \quad = -\frac{k_1}{\sqrt{\pi \alpha_1 (t + t_0)}}. \tag{35}$$

With known initial data, the reconstructed results corresponding to $\delta = 0$, $\delta = 1\%$, and $\delta = 5\%$ are shown in Figs. 10, 11, and 12, respectively, whereas Figs. 13, 14, and 15, respectively, represent the same in the case of unknown initial data. To the best of our knowledge, the task of simultaneous reconstruction of the boundary and initial data for this benchmark has not been considered in the MFS literature, which is why we do not provide a comparison against other literature data.

4.4. Summary of observations for Examples 1 and 2

The noise in the Dirichlet data (16) induces more noise in the computations in the liquid phase, as the Stefan conditions (7) and (8) are collocated on the approximated free boundary. Despite this, the accuracy in the retrieved boundary and initial data appears to be quite good for both of the test problems. More importantly, the order of error is the

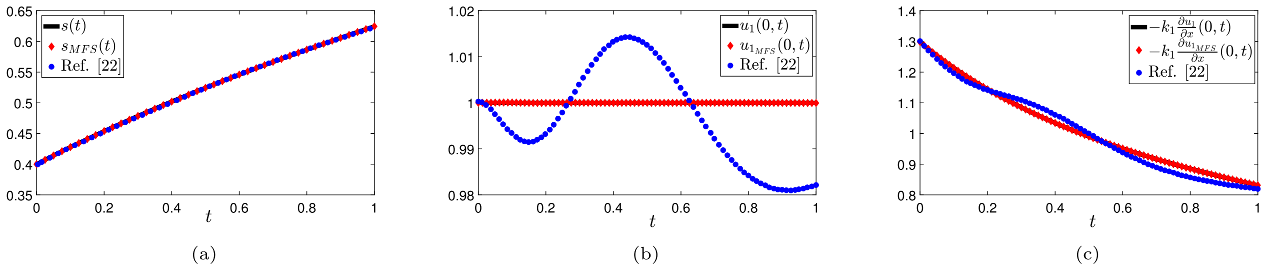

Fig. 10. Approximations obtained for Example 2 and $\delta = 0$, when the initial conditions (3) and (4) are prescribed. $\mathcal{N}_2^* = 72$, $h_2^* = 2.5$, $\lambda_2^* = 10^{-14}$, $\mathcal{N}_1^* = 56$, $h_1^* = 2.0$, $\lambda_1^* = 10^{-11}$. The approximations in [22] were obtained with $\mathcal{N}_1 = \mathcal{N}_2 = 160$, $h_1 = h_2 = 2$, $\lambda_1 = \lambda_2 = 10^{-12}$. The total number of collocation points therein is 444.

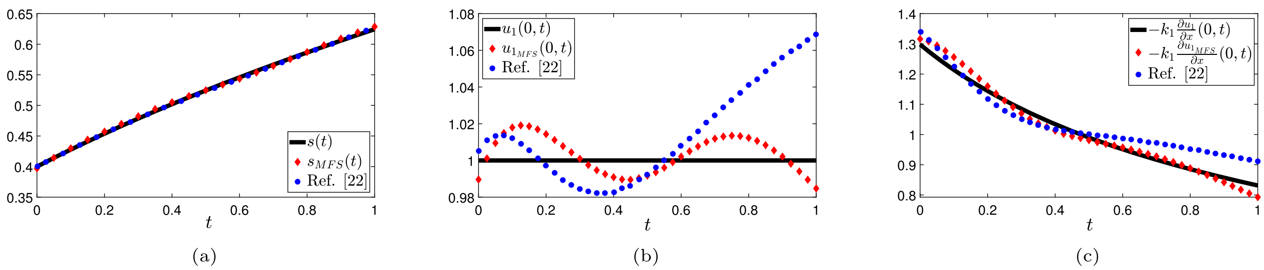

Fig. 11. Approximations obtained for Example 2 and $\delta = 1\%$, when the initial conditions (3) and (4) are prescribed. $\mathcal{N}_2^* = 76$, $h_2^* = 1.9$, $\lambda_2^* = 10^{-4}$, $\mathcal{N}_1^* = 40$, $h_1^* = 1.0$, $\lambda_1^* = 10^{-2}$. The approximations in [22] were obtained with $\mathcal{N}_1 = \mathcal{N}_2 = 80$, $h_1 = h_2 = 2$, $\lambda_1 = \lambda_2 = 10^{-6}$. The total number of collocation points therein is 224.

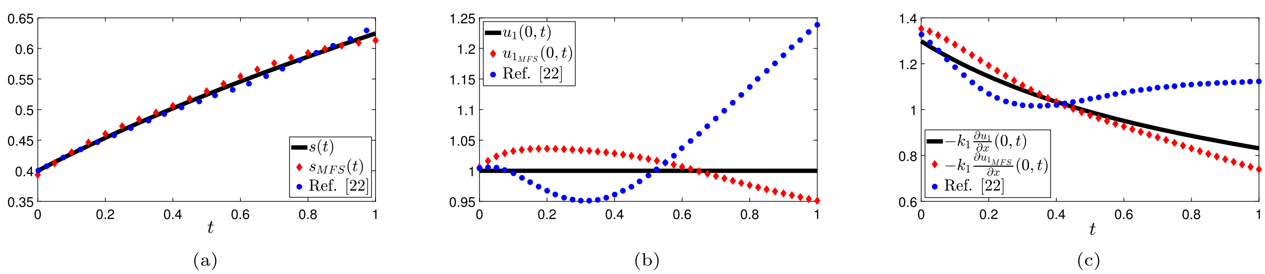

Fig. 12. Approximations obtained for Example 2 and $\delta = 5\%$, when the initial conditions (3) and (4) are prescribed. $\mathcal{N}_2^* = 56$, $h_2^* = 2.2$, $\lambda_2^* = 10^{-4}$, $\mathcal{N}_1^* = 12$, $h_1^* = 1.3$, $\lambda_1^* = 10^{-5}$. The approximations in [22] were obtained with $\mathcal{N}_1 = \mathcal{N}_2 = 80$, $h_1 = h_2 = 2$, $\lambda_1 = \lambda_2 = 10^{-6}$. The total number of collocation points therein is 224.

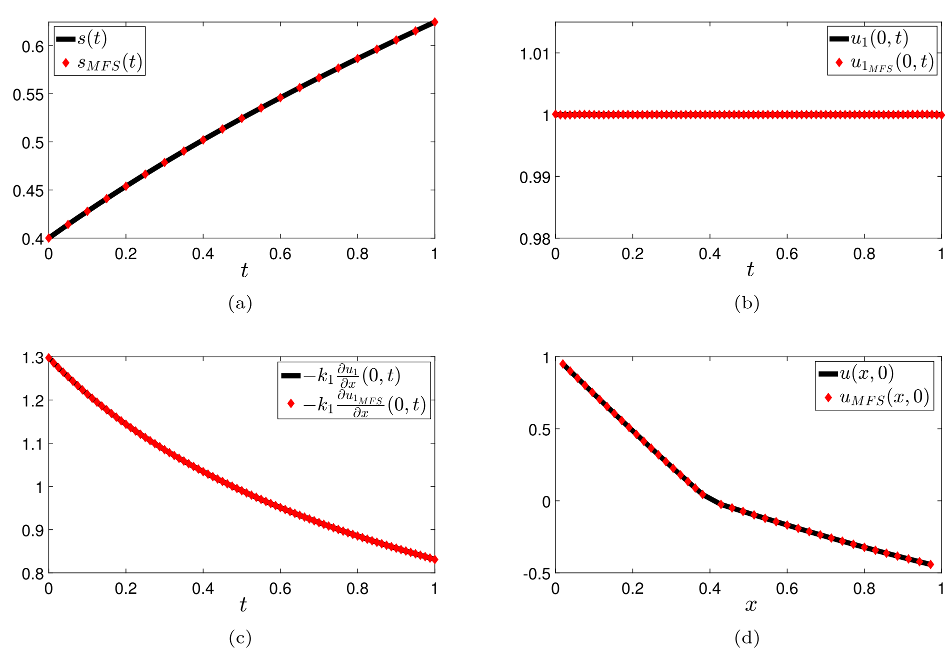

Fig. 13. Approximations obtained for Example 2 and $\delta = 0$, when the initial conditions (3) and (4) are not prescribed. $\mathcal{N}_2^* = 76$, $h_2^* = 2.5$, $\lambda_2^* = 10^{-16}$, $\mathcal{N}_1^* = 80$, $h_1^* = 1.4$, $\lambda_1^* = 10^{-12}$.

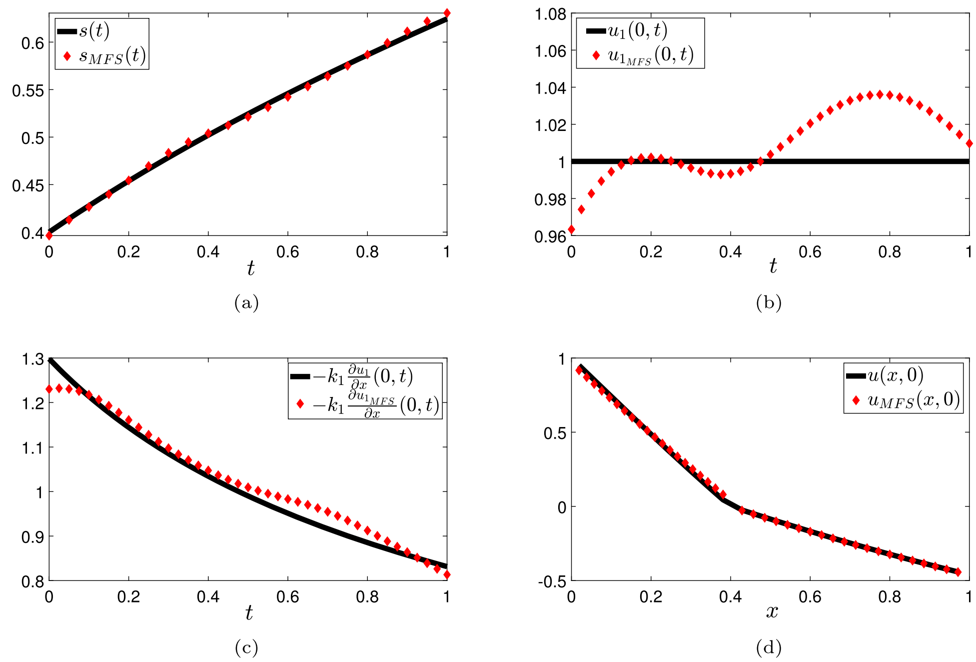

Fig. 14. Approximations obtained for Example 2 and $\delta = 1\%$, when the initial conditions (3) and (4) are not prescribed. $\mathcal{N}_2^* = 60$, $h_2^* = 2.1$, $\lambda_2^* = 10^{-6}$, $\mathcal{N}_1^* = 80$, $h_1^* = 1.0$, $\lambda_1^* = 10^{-1}$.

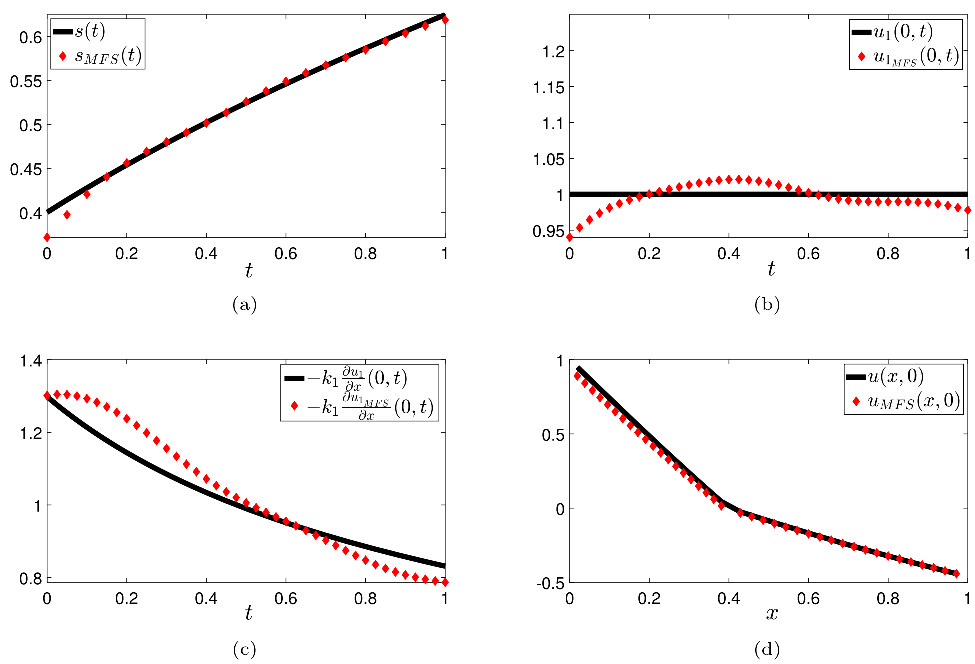

Fig. 15. Approximations obtained for Example 2 and $\delta = 5\%$, when the initial conditions (3) and (4) are not prescribed. $\mathcal{N}_2^* = 44$, $h_2^* = 1.3$, $\lambda_2^* = 10^{-3}$, $\mathcal{N}_1^* = 56$, $h_1^* = 1.3$, $\lambda_1^* = 10^{-1}$.

same as that of the noise that is input into the computations. However, it is noteworthy that the heat flux data on Γ_1^1, which is quite challenging to reconstruct, has been recovered with reasonable accuracy, even with high noise levels. A further observation is that the approximations improve as the noise level is reduced, as expected.

Through comparison in Figs. 4-12, we observe that the adopted method reconstructs the data better than the composite optimization [22]. Furthermore, for the same noise level, the proposed method seems to be computationally competitive, in terms of the numbers of source and collocation points alone, with the composite one based on nonlinear optimization that was developed in [22]. However, we believe that the advantage of our method is that it finds the optimal MFS and regularization parameters in a systematic and efficient way; being able to do this eliminates any trial-and-error attempt to find these parameters, and therefore ultimately reduces computation time.

For the second example, the behaviour of error with respect to the number of source points or, in other words, the number of basis functions in the MFS approximation is also studied. For $\delta = 0$ with known initial data (3) and (4), we plot in Fig. 16 the root-mean-square error in u_1, denoted by $RMSEu_1$, against the number of source points, $\mathcal{N}$. The values of $\mathcal{N}$ are chosen between 16 and 56, inclusively, in increments of 8. Note that the error in u_1 shown herein is monotonically

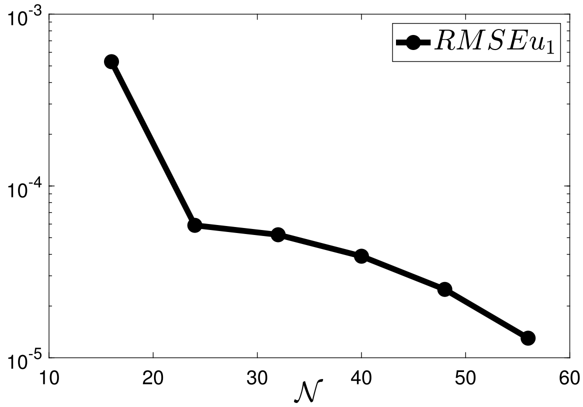

Fig. 16. Root-mean-square error in u_1, $RMSEu_1$, for Example 2 without noise.

decreasing. We may also observe similar patterns in error computed in the supremum norm and the inverse problem with unknown initial data (3) and (4). However, we would like to point out that such behaviour in the error might be merely due to a particular placement of the source and collocation points. We may not expect such monotonic behaviour for a different arrangement of points with noisy data. The curve for $RMSEu_1$ may shift either upwards or downwards while preserving its current shape based upon the accuracy of the obtained s_{MFS} from the solid phase.

Finally, we point out that, although it may appear from Figs. 10-15 easier to reconstruct Neumann data than Dirichlet data in Example 2, this is not actually the case; it only appears to be so because of the scales in the plots, since the Dirichlet data that we are trying to reconstruct is a constant.

5. Conclusion

In this article, a phase-wise split approach was proposed to solve an inverse two-phase nonlinear Stefan problem for the first time in the MFS literature or otherwise. Moreover, numerical investigation for two benchmark examples demonstrated the robustness and efficiency of the adopted method. Furthermore, this method opens up the possibility of linear MFS discretizations and, therefore, a more systematic way to choose the parameters required for MFS, i.e. the locations of the source and collocation points.

A number of future research directions are now possible. One involves three-phase problems [35–37], which also arise in casting processes; in addition to the solid and melt phases, there is a mushy zone located between them in which solid and melt phases can coexist [38,39]. An alternative direction would be higher-dimensional two-phase nonlinear inverse Stefan and Cauchy-Stefan problems; as mentioned earlier, a two-dimensional problem of this kind was considered in [24], although this was of design-type, in which the location of the moving boundary is prescribed.

Link to the Reproducible Capsule

https://codeocean.com/capsule/9072139/tree

Acknowledgement

The first two authors would like to thank SERB, India for the financial support received via Grant Number SRG/2019/001973. Further, they also acknowledge DST, New Delhi, India, for providing facilities through DST-FIST lab, Department of Mathematics, BITS-Pilani, Hyderabad Campus, where part of this work was carried out.

References

[1] M. Farid, A unified approach to the heat and mass transfer in melting, solidification, frying and different drying processes, Chem. Eng. Sci. 56 (18) (2001) 5419–5427.
[2] D. Słota, Restoring boundary conditions in the solidification of pure metals, Comput. Struct. 89 (1–2) (2011) 48–54.
[3] S. Chen, B. Merriman, S. Osher, P. Smereka, A simple level set method for solving Stefan problems, J. Comput. Phys. 135 (1) (1997) 8–29.
[4] M. Davis, P. Kapadia, J. Dowden, Solution of a Stefan problem in the theory of laser welding by the method of lines, J. Comput. Phys. 60 (3) (1985) 534–548.
[5] M. Storti, Numerical modeling of ablation phenomena as two-phase Stefan problems, Int. J. Heat Mass Transf. 38 (15) (1995) 2843–2854.
[6] L. Rubinstein, The Stefan problem: comments on its present state, IMA J. Appl. Math. 24 (3) (1979) 259–277.
[7] J.M. Hill, Y.H. Wu, On a nonlinear Stefan problem arising in the continuous casting of steel, Acta Mech. 107 (1) (1994) 183–198.
[8] J. Mahmoudi, M. Vynnycky, P. Sivesson, H. Fredriksson, An experimental and numerical study on the modelling of fluid flow, heat transfer and solidification in a copper continuous strip casting process, Mater. Trans. 44 (9) (2003) 1741–1751.
[9] J.F. Rodrigues, F. Yi, On a two-phase continuous casting Stefan problem with nonlinear flux, Eur. J. Appl. Math. 1 (3) (1990) 259–278.
[10] M. Vynnycky, A mathematical model for air-gap formation in vertical continuous casting: the effect of superheat, Trans. Ind. Inst. Metals 62 (2009) 495–498.
[11] M. Vynnycky, On the onset of air-gap formation in vertical continuous casting with superheat, Int. J. Mech. Sci. 73 (2013) 69–76.
[12] S.L. Mitchell, M. Vynnycky, On the accurate numerical solution of a two-phase Stefan problem with phase formation and depletion, J. Comput. Appl. Math. 300 (2016) 259–274.
[13] B.J. Florio, M. Vynnycky, S.L. Mitchell, S.B.G. O'Brien, On the interactive effects of mould taper and superheat on air gaps in continuous casting, Acta Mech. 228 (2017) 233–254.
[14] S.L. Mitchell, M. Vynnycky, Verified reduction of a model for a continuous casting process, Appl. Math. Model. 48 (2017) 476–490.
[15] V. Barbu, Boundary controllability of phase-transition region of a two-phase Stefan problem, Syst. Control Lett. 150 (2021) 104896.
[16] L. Bougoffa, R.C. Rach, A. Mennouni, On the existence, uniqueness, and new analytic approximate solution of the modified error function in two-phase Stefan problems, Math. Methods Appl. Sci. 44 (2021) 10948–10956.
[17] S. Akhtar, M. Xu, A.P. Sasmito, Development and validation of an asymptotic solution for a two-phase Stefan problem in a droplet subjected to convective boundary condition, Int. J. Therm. Sci. 164 (2021) 106923.
[18] D. Słota, Homotopy perturbation method for solving the two-phase inverse Stefan problem, Numer. Heat Transf., Part A, Appl. 59 (10) (2011) 755–768.
[19] N. Gol'dman, Inverse Stefan Problems, vol. 412, Springer Science & Business Media, 2012.
[20] E. Hetmaniok, I. Nowak, D. Słota, A. Zielonka, Determination of optimal parameters for the immune algorithm used for solving inverse heat conduction problems with and without a phase change, Numer. Heat Transf., Part B, Fundam. 62 (6) (2012) 462–478.
[21] A. Karageorghis, D. Lesnic, L. Marin, A survey of applications of the MFS to inverse problems, Inverse Probl. Sci. Eng. 19 (3) (2011) 309–336.
[22] B.T. Johansson, D. Lesnic, T. Reeve, A meshless method for an inverse two-phase one-dimensional nonlinear Stefan problem, Math. Comput. Simul. 101 (2014) 61–77.
[23] B.T. Johansson, D. Lesnic, T. Reeve, A meshless method for an inverse two-phase one-dimensional linear Stefan problem, Inverse Probl. Sci. Eng. 21 (1) (2013) 17–33.
[24] B.T. Johansson, D. Lesnic, T. Reeve, A meshless regularization method for a two-dimensional two-phase linear inverse Stefan problem, Adv. Appl. Math. Mech. 5 (6) (2013) 825–845.
[25] D.A. Murio, Solution of inverse heat conduction problems with phase changes by the mollification method, Comput. Math. Appl. 24 (7) (1992) 45–57.
[26] J.R. Cannon, J. Douglas Jr., The Cauchy problem for the heat equation, SIAM J. Numer. Anal. 4 (3) (1967) 317–336.
[27] A. El Badia, F. Moutazaim, A one-phase inverse Stefan problem, Inverse Probl. 15 (6) (1999) 1507–1522.
[28] P. Manselli, S. Vessella, On continuous dependence, on noncharacteristic Cauchy data, for level lines of solutions of the heat equation, Forum Math. 3 (3) (1991) 513–522.
[29] T. Wei, M. Yamamoto, Reconstruction of a moving boundary from Cauchy data in one-dimensional heat equation, Inverse Probl. Sci. Eng. 17 (4) (2009) 551–567.
[30] C.D. Hill, Parabolic equations in one space variable and the non-characteristic Cauchy problem, Commun. Pure Appl. Math. 20 (3) (1967) 619–633.
[31] Y.B. Wang, J. Cheng, J. Nakagawa, M. Yamamoto, A numerical method for solving the inverse heat conduction problem without initial value, Inverse Probl. Sci. Eng. 18 (5) (2010) 655–671.
[32] G.M.M. Reddy, M. Vynnycky, J.A. Cuminato, On efficient reconstruction of boundary data with optimal placement of the source points in the MFS: application to inverse Stefan problems, Inverse Probl. Sci. Eng. 26 (9) (2018) 1249–1279.
[33] G.M.M. Reddy, M. Vynnycky, J.A. Cuminato, An efficient adaptive boundary algorithm to reconstruct Neumann boundary data in the MFS for the inverse Stefan problem, J. Comput. Appl. Math. 349 (2019) 21–40.

[34] G.M.M. Reddy, P. Nanda, M. Vynnycky, J.A. Cuminato, An adaptive boundary algorithm for the reconstruction of boundary and initial data using the method of fundamental solutions for the inverse Cauchy–Stefan problem, Comput. Appl. Math. 40 (3) (2021) 99.
[35] D. Słota, Using genetic algorithms for the determination of an heat transfer coefficient in three-phase inverse Stefan problem, Int. Commun. Heat Mass Transf. 35 (2) (2008) 149–156.
[36] R. Grzymkowski, D. Słota, Numerical method for multi-phase inverse Stefan design problems, Arch. Metall. Mater. 51 (2006) 161–172.
[37] M. Slodička, H. De Schepper, Determination of the heat-transfer coefficient during solidification of alloys, Comput. Methods Appl. Mech. Eng. 194 (2005) 491–498.
[38] M. Vynnycky, S. Saleem, On the explicit resolution of the mushy zone in the modelling of the continuous casting of alloys, Appl. Math. Model. 50 (2017) 544–568.
[39] M. Assunção, M. Vynnycky, S.L. Mitchell, On small-time similarity-solution behaviour in the solidification shrinkage of binary alloys, Eur. J. Appl. Math. 32 (2021) 199–225.